

Advancing Local Distance Discrimination of Explosions and Earthquakes with Joint P/S and M_L - M_C Classification

Ruijia Wang^{1,2}, Brandon Schmandt¹, Monique Holt^{3,4}, and Keith Koper³

1. Department of Earth and Planetary Sciences, University of New Mexico, Albuquerque, NM, US
2. Department of Earth and Space Sciences, Southern University of Science and Technology, Shenzhen, Guangdong, China
3. Department of Geology and Geophysics, University of Utah, Salt Lake City, Utah, US
4. Department of Earth and Environmental Sciences, University of Illinois at Chicago, Chicago, Illinois, US

Corresponding author: ruijia.wang@ualberta.ca

Key points:

1. P/S ratio and M_L - M_C exhibit complementary sensitivity for discriminating earthquakes and single-fired explosions.
2. Excellent classification performance is achieved in four diverse tectonic settings without local site corrections.
3. The new methodology will improve the ability to identify low-yield underground explosions.

Key words:

Local-regional earthquakes; Explosive sources; Seismic source classification; U.S continent; Body wave ratios; Local and coda magnitudes

Abstract

Classification of local-distance, low-magnitude seismic events is challenging because signals can be numerous and difficult to characterize with approaches developed for larger magnitude events observed at greater distances. Yet, accurate classification is important to studies of earthquake processes and detection of potential underground nuclear tests. Here, we combine two classification metrics: the three-component ratio of high-frequency P/S amplitudes and the difference between local and coda duration magnitudes (M_L - M_C). The metrics use different parts of the high-frequency wavefield and exhibit complementary sensitivity for classification of $M \sim 0.5$ –4 natural earthquakes and borehole explosions, which are the best analog for underground nuclear explosions. Using means from bootstrap resampling across four diverse geologic settings, joint classification achieves >94.4% true positives and <8.4% false positives when using ≥ 8 seismographs within 200 km. This high performance is obtained without

local site corrections, indicating that the method may be transportable for local event classification.

Plain-Language Summary

Separating explosive sources from earthquakes is fundamental to seismic monitoring and seismic hazard evaluation. Many methods have been developed to discriminate between the two types of events, mostly taking advantage of depth differences and/or the energy ratios between seismic phases. However, these methods may be less effective at local scales (i.e., <200 km) and discrimination parameters often need to be calibrated to adapt to various regional settings. In this study, we collected hundreds of $M\sim 0.5\text{--}4$ earthquakes and borehole explosions from four regions in the western U.S. and tested two popular discrimination methods: 1) body-wave energy ratio (P/S) and 2) magnitude differences ($M_L - M_C$). We find the two metrics complement each other, providing better discrimination in all four regions with station numbers as low as ~ 8 . Furthermore, the joint method shows less dependence on local crustal setting, thus, it may be applicable to new regions with complex geological settings or scarce calibration data.

1 Introduction

Accurate classification of explosive seismic sources and earthquakes is a key component for agencies monitoring compliance with nuclear test ban treaties (e.g., Bowers & Selby, 2009) and for hazard mitigation agencies monitoring earthquake activity (e.g., Renouard *et al.*, 2021). Seismic discrimination of underground explosions has been successful for larger magnitude events that are typically observed at teleseismic distances (i.e., >3,000 km), however discrimination at local distances (< 200 km) remains challenging. Unidentified explosions can bias earthquake statistics and increase uncertainty of seismic hazard prediction (Mackey *et al.*, 2003; Astiz *et al.*, 2014; Gulia & Gasperini, 2021; Marzen *et al.*, 2021). Furthermore, mining blasts (Dokht *et al.*, 2020) and underground weapons tests (Tian *et al.*, 2018; Walter *et al.*, 2018) may temporarily increase regional seismic hazard via activation of local faults or collapse events (Walter *et al.*, 2018). Thus, discrimination of small explosions and earthquakes at local distances remains crucial. However, adaptation of teleseismic methods to local scales and smaller magnitudes is challenged by factors like weaker and higher-frequency seismic phases, highly variable geological structures, and limited station coverage (Taylor *et al.*, 1989; Hartse *et al.*, 1997; O’Rourke *et al.*, 2016).

Local-scale source classification, including machine-learning based techniques (e.g., Linville *et al.*, 2019), relies more on high frequency body wave measure-

ments such as P/S ratios because long period surface waves are barely excited by small magnitude events (e.g., Taylor *et al.*, 1989; Kim *et al.*, 1993; O’Rourke & Baker, 2017; Walter *et al.*, 2018). Accordingly, depth-sensitive magnitude-based screening metrics, like the difference between local and coda duration magnitudes (M_L-M_C), have been proposed and successfully applied to several regions (Zeiler & Velasco, 2009; Holt *et al.*, 2019; Voyles *et al.*, 2020; Koper *et al.*, 2021), replacing the difference between teleseismic body wave and surface wave magnitudes ($m_b:M_S$) that is commonly used for larger events (Stevens & Day, 1985; Russell, 2006; Selby *et al.*, 2012). Although both methods mentioned above show potential for local-scale discrimination, empirical corrections from global-to-regional studies may be difficult to adapt to local crustal wave propagation (Walter *et al.*, 1995; Walter & Taylor, 2001; Anderson *et al.*, 2009). Such corrections and regional calibrations usually rely on high-resolution structure models and/or sufficient pre-classified events for learning (e.g., Fisk *et al.*, 1996; Rabin *et al.*, 2016). Furthermore, region-specific calibration requirements degrade the transportability of discrimination methods (Douglas, 2007).

The rapid growth of local-to-regional seismic data in recent years motivates revisiting classic waveform-based discrimination methods at local distances (O’Rourke *et al.*, 2016; Pyle & Walter, 2019; Wang *et al.*, 2020; Koper *et al.*, 2021). In this study, we systematically calculated P/S ratio and M_L-M_C values for earthquakes and borehole explosives recorded at distances < 200 km by dozens of seismometers in four distinct regions. Uniform processing for four local-distance datasets enables more direct comparison than is possible among prior studies using variable processing workflows and distance ranges. Performance of our joint metric is evaluated by systematically decreasing station coverage for individual and merged datasets to simulate a variety of more realistic monitoring conditions. We show that accurate discrimination could be achieved with minimal local knowledge (i.e., an approximate 1-D velocity model) and the joint method is transportable across various local-regional settings.

2 Datasets

We aim to collect local seismic observations of single-fired explosive sources and earthquakes at comparable scales but variable tectonic settings. Toward this goal, four datasets in the U.S. are used (Figure 1): Mount St. Helens magma imaging project (MSH) in Washington, the Bighorn Arch Seismic Experiment (BASE) in Wyoming, the Source Physics Experiment 1 (SPE) in Nevada, and the Salton Seismic Imaging Project (SSIP) in California. As borehole shots are effective proxies for underground nuclear tests (Stump *et al.*, 2002), we focus on a binary discrimination between borehole shots and earthquakes (i.e., mine blasts from BASE are excluded). The four datasets contain 90 borehole shots and ~ 290 earthquakes with comparable magnitudes and event-station distances, which are concentrated at < 200 km (Figure S1).

2.1 Mount St. Helens (MSH)

Nearly 90 broadband stations recorded 23 explosive sources (M_L 0.9–2.3) and 91 earthquakes (M_L 1.5–3.3, as reported by USGS) within 75 km of the volcano during the 2014–2016 iMUSH project (Figure 1a; Han *et al.*, 2016, Ulberg *et al.*, 2020). The explosive events are shallow borehole shots with explosive loads of either 454 or 907 kg, forming a relatively uniform distribution around the volcano. Earthquakes (depth < 20 km) in this region are broadly distributed as well, with slightly more events located in the St. Helens seismic zone and West Rainier seismic zone (Figure 1a; Stanley *et al.*, 1996).

2.2 Bighorn Arch Seismic Experiment (BASE)

The BASE project was conducted in 2010 to image the Bighorn Arch (Figure 1b; Worthington *et al.*, 2016). The dataset contains 21 explosive sources (M_L 0.7–1.7; loads 113–907 kg), 19 earthquakes (M_L 0.3–2.7), and 37 mine blasts (M_L 1.8–3.3) recorded by ~90 broadband stations and ~180 short-period stations. Most mine blasts are located to the southeast of the array with potential loads on the order of 10,000 kg (O’Rourke *et al.*, 2016). P/S ratio and M_L - M_C results for the mine blasts in BASE are shown in Figure 2 for readers’ interest.

2.3 Source Physics Experiment Phase 1 (SPE)

Five borehole shots (M_L 1.2–2.1, loads 90–5,035 kg) are available for SPE Phase 1 in 2011, which occurred in the area of prior underground nuclear explosion tests in the U.S. (Figure 1c; Snelson *et al.*, 2013). They are fired at the same location at the center of the array with variable depths (see Figure 1c). The station coverage of these events ranges from ~3–35, which makes it the smallest among the four datasets. We used 110 earthquakes (M_L 1.0–4.4) that occurred in the area during or after 2011.

2.4 Salton Sea Imaging Project (SSIP)

SSIP conducted an active source seismic survey in 2011 to image crustal faults and constrain rifting processes (Figure 1d; Han *et al.*, 2016; Fuis *et al.*, 2017). Up to ~80 broadband stations were available during SSIP in 2011 and 126 explosions were single-fired with loads ranging from 3 to 1,440 kg. To ensure a comparable magnitude to earthquakes and the other 3 datasets, we only used 41 shots with loads >200 kg (M_L 0.6–2.1). The USGS catalog returns 76 events (M_L 1–3.6) during the month, including 6 borehole shots mis-cataloged as earthquakes (Table S1). The remaining earthquakes are mostly located within Mexico along the Imperial Fault Zone, potential aftershocks of the M7.2 Baja California earthquake (e.g., Castro *et al.*, 2011).

3 Methods

3.1 P/S ratio analysis

Four regional 1-D velocity models are used to predict the P or S phase arrivals of events at the corresponding datasets (Figure S2). All broadband or high gain three-component records are filtered between 10–18 Hz because that was found to be optimal for local-distance P/S discrimination by Wang *et al.* (2020). The P/S ratios are then calculated from the effective variance of given phases using Eq (1).

$$P/S = \frac{\sqrt{(P_R^2 + P_T^2 + P_Z^2) - (N_R^2 + N_T^2 + N_Z^2)}}{\sqrt{(S_R^2 + S_T^2 + S_Z^2) - (N_R^2 + N_T^2 + N_Z^2)}}, \text{ Eq (1)}$$

where, R, T, Z denotes the radial, transverse, and vertical component recordings for P-, S- and noise (N) windows, respectively. Three-component SNRs are also calculated using the same P windows and noise windows 10 sec before P arrival. A consistent cutoff of $\text{SNR} > 2$ is required for a valid P/S ratio of the given event-station pair. Considering the distance ranges, no pre-S noise is involved, as the P-coda may continue until the S-wave arrival. Therefore, our SNR threshold purposely admits events with low S amplitudes. No site correction (e.g., MDAC, Walter & Taylor, 2001) is applied and the final event-based P/S ratio is determined from the median value of all stations with valid P/S ratio measurements. The final P/S ratios are calculated with only 1-D velocity models and earthquake/explosive catalogs as inputs. More details on parameters and comparison to methods from previous studies are provided in Text S2.

3.2 M_L - M_C

M_L and M_C values for all events are calculated from the waveforms; none of the M_L values are adopted from the USGS or local monitoring catalogs. Thus, all magnitude calculations are conducted without prior information of source type. To emulate the situation that might exist when testing begins in a new region, a consistent calibration of both M_L and M_C (optimized for Utah) is applied to all datasets (e.g., Koper *et al.*, 2021).

When calculating M_L , the regional broadband seismic records (i.e., HH and BH components) are first converted to Wood-Anderson seismometer equivalent response. The station amplitude is then measured from the two horizontal-components without station corrections and distance corrections are applied (e.g., Richter, 1958).

For M_C calculation, the formula inherits the current duration magnitude definitions of UUSS (Pechmann *et al.*, 2006) with a modified cutoff threshold ($\text{SNR}=2$). All vertical components of high gain seismometers are corrected for instrument response and filtered between 1–10Hz. The seismogram envelopes

are generated for coda windowing, which starts near the maximum S-wave amplitude and ends with the designated SNR cutoff. The M_C at a station is then calculated from the measured coda duration using the equations described in Koper *et al.* (2021). Note that the SNRs here are from single (vertical) components, different from the three-component SNR used for P/S ratio at higher frequencies (10–18 Hz). For both M_L and M_C measurements, the final event magnitudes are determined as the median from >3 valid station-based measurements.

3.3 Performance evaluation using ROC curve and Mahalanobis distance

The best threshold values for source type classification with either P/S ratio or M_L - M_C are obtained via grid searches to optimize the Area Under the Curve (AUC) defined by the Receiver Operating Characteristic (ROC). The ROC curve (Figure S5) jointly considers the true positive rate (TPR) and false positive rate (FPR) for binary classification (Fawcett, 2006). In our case, the explosions are defined as “positive”, and earthquakes are defined as “negative”. Such evaluation is event-based, where the median value of the P/S ratio or M_L - M_C from all valid stations (>3) is determined as the final value for that event. In the joint domain, the best cutoff line is also obtained by grid searching using a 2-D parameter space of slope and intercept to maximize the AUC (Figure S6).

When all the events are finalized with a combination of P/S ratio and M_L - M_C , the Mahalanobis distance (Δ^2) between two types of events is calculated using the mean and covariance values. The distances do not hold any specific physical meaning but are often used as a mathematical evaluation to define the “closeness” of two populations in a given parameter space (i.e., P/S ratio and M_L - M_C). We refer readers to the supporting materials and previous publications for details (e.g., Tibi, 2021). In general, AUC evaluates a discrimination that has been performed on known datasets, whereas Mahalanobis distances could reflect the robustness of the discriminations that may transfer to future applications.

4 Results

4.1 Individual metrics

Among the four different settings, the optimal P/S ratio and M_L - M_C cutoffs vary between 0.9–1.5 and -0.15–0.3, respectively (Figure 2). The best P/S ratio cutoffs are comparable between regions (~ 1) and highest for SPE. BASE requires the lowest individually optimized P/S ratio cutoff (0.9–1.1 achieve identical performance) but the highest M_L - M_C cutoff (0.3). For all four datasets, P/S ratios provide more robust discrimination than M_L - M_C based on TPR (recall) and FPR, which were used to optimize the discrimination threshold. Precision (i.e., true positives/total positives) is also given as an additional performance measure (Table 1). For MSH, BASE and SPE, optimal P/S ratio cutoffs could

identify the explosions with only a few false alarms, whereas M_L - M_C results in higher FPR. The precision (0.6 and 0.23) is low for both metrics at SPE, as only three explosives meet our quality control (i.e., low station coverage). In addition, we did not observe apparent distance-dependence of P/S ratios from the four datasets at <200 km (Text S2 and Figure S3). As short period stations are used for P/S calculations, whereas M_L - M_C requires broadband stations, most events across the four datasets have a higher number of valid stations for P/S ratio than for M_L - M_C (Figure S5).

4.2 Joint method

A total of 68 explosives and 262 earthquakes were analyzed with a minimum magnitude of 0.6 and 0.7, respectively. The two groups are well-separated in the joint P/S and M_L - M_C domain (Figure 2). The best joint cutoffs are determined from grid-searching over slopes and intercepts (Figure S6) and the optimal values are reported in Table 1. For individual datasets, a wide range of slopes (~0.7–2.5) are acceptable except for SSIP (see Figure S6), suggesting a comparable contribution from both methods. The low slope value obtained for SSIP is likely affected by the single explosion with P/S ratio <1 (Figure 2d). Overall, the joint method achieves better performance for all four datasets (Table 1), leading to TPR=100% and FPR<1.2%. For regions that P/S ratio alone achieved TPR=100%, the joint method increases precision by ~15% (i.e., MSH and SPE) by rejecting more false positives.

Compared to earlier studies of local to regional seismic source discrimination (e.g., Bennett *et al.*, 1986), the performance of our joint discrimination approach benefits from dense station coverage in the four study regions (see Figure 1). Thus, we tested the station-coverage effect via bootstrapping: a given number of stations are randomly selected (without repetition) and we require no SNR threshold. In other words, valid stations are often less than the total number of stations used within each trial to simulate the realistic circumstance in which not all stations have adequate SNR for a specific event. For each total number of stations, random selection is repeated 1,000 times and the mean (and standard deviation) of the TPR and FPR are recorded (Figure 3). As expected, the discrimination performance increases with station coverage and larger variations are observed when a dataset contains fewer events (e.g., SPE). Meanwhile, decent TPR (64.4%–94.5%) and FPR (5.8%–22.2%) could be achieved with 8 stations. Improvement is limited (<5%) with >32 stations.

5 Discussion

The joint method demonstrates promising transportability for uniformly processed datasets. Although the discrimination thresholds vary between regions—especially for M_L - M_C —the explosive sources and earthquakes always fall into two clusters in the P/S versus M_L - M_C domain. Surprisingly, such separation is preserved even after merging all four datasets: the covariance ellipses remain

separated at 1 standard deviation (Figure 4a). Similarly high TPR (>95%) and low FPR (<5%) are achieved when a joint cutoff line is used rather than individually optimized cutoffs for each array, leading to a maximum AUC=0.9755 (Figure 4b). In fact, such discrimination performance can be achieved with fewer stations, for example, 8-stations leads to averaged TPR=94.4% and FPR=8.4% (Figure 4c) with <5% variations for both, comparable to the performance of supervised machine-learning (e.g., Reynen & Audet, 2017). In addition, our approach is particularly effective for identifying the true explosives, with only 1 out of 66 borehole shots resulting in a false negative classification.

The Mahalanobis distance (and minimum probability of mis-classification P_M ; Text S4) between the two populations increases (decreases) to 18.5 (1.6%) in the joint domain, whereas P/S and M_L - M_C result in 15.4 (2.5%) and 2.6 (21.1%), respectively. Such improvement could be explained by three types of complementary sensitivities between P/S and M_L - M_C : frequency, depth, and distance. First, the two methods focus on different frequency ranges, with P/S ratios calculated at 10–18 Hz, M_C at 1–10 Hz and M_L at <1.25 Hz. Second, previous studies suggested that M_L - M_C screening is sensitive to event depth because shallow events create stronger coda (Holt *et al.*, 2019), while P/S ratio exhibits less sensitivity to depth at local distances (Wang *et al.*, 2020). Lastly, the depth-sensitivity of M_L - M_C is more effective at near-distances, evidenced by increased slope of the “combined” discrimination threshold line reflecting higher contribution from M_L - M_C (Figure 4d). In addition, when restricting the combined dataset to near distances, the relatively low Mahalanobis distances imply worse separation between the two populations (Figure 4d), echoing the reduced performance of P/S-ratio based discrimination near the source in some prior studies (e.g., O’Rourke *et al.*, 2016, Pyle & Walter, 2019). We speculate that such near-distance challenges may partly reflect poorer station coverage, which diminishes at distances at ~60 km for the four datasets (Figure S1). Regardless of the root factor that challenges near-source P/S-ratio-based discrimination, adding M_L - M_C measurements leads to a stable and high AUC (>0.95) across all distances.

The success of our joint discrimination is somewhat influenced by data selection, in which any events missing any of the three measurements (i.e., P/S ratio, M_L , and M_C) are excluded from the classification test. As a result, 23 earthquakes and 21 explosive events were not analyzed in the joint domain. However, we note that all explosions can still be discriminated by P/S ratio alone (i.e., P/S>1), albeit with a higher FPR (26%) than we found for the events included in the joint analysis (e.g., Figure S9, also see Table S1). Therefore, the high performance achieved by our joint discrimination is not strongly biased by the quality controls governing data selection.

Unlike previous locally specific discrimination studies that demand site (e.g., Wang *et al.*, 2021), path (e.g., Rodgers *et al.*, 1999) and/or magnitude corrections (e.g., Walter *et al.*, 1995), the joint method as implemented here does not rely on locally-specific pre- or post-measurement corrections. Our discrim-

ination requires no statistical priors such as the ratio or number of explosives expected. The only prerequisites are three-component data and an approximate 1-D velocity model for phase windowing. Encouraging performance without local correction factors does not imply that such corrections are unimportant. In regions where sufficient data exist to calibrate local corrections, we expect that incremental but important improvements in performance are possible for a given number of stations (e.g., Wang *et al.*, 2020; Kintner *et al.*, 2020). Lastly, both methods used here are fast to calculate, making the joint method practical for near-real time screening at local scale (e.g., Dempsey *et al.*, 2020, Scafidi *et al.*, 2018).

Joint discrimination could also benefit future development of new discrimination methods, including machine-learning based techniques. The success of our application offers unique insight into the “black-box” classification resulting from machine-learning-based discrimination algorithms by highlighting specific parts of the wavefield that are diagnostic of different source types (e.g., Kortström *et al.*, 2016; Linville *et al.*, 2019; Renouard *et al.*, 2021). The high-transportability of our method may also mitigate potential challenges with network-based discriminations, where location pattern recognition or site-specific source effects could unintentionally dominate source type determination. For instance, a neural network could learn to associate explosive sources with a specific place if event location is included in end-to-end classification process along with other information such as waveforms or spectrograms (e.g., Reynen & Audet, 2017; Tang *et al.*, 2020). Our results suggest that attributes such as P/S ratios and M_L - M_C could be beneficial to include for training future classification models.

6 Conclusion

We applied P/S ratio analysis and M_L - M_C calculations to four regional datasets with ~ 400 small-moderate sized earthquakes and explosions recorded by tens-to-hundreds of stations concentrated at distances < 200 km. The joint method requires minimal processing and little prior knowledge of site or path conditions. Joining the two discrimination methods achieves high accuracy in source type classification with individual dense local arrays (up to TPR=100% and FPR=0% when large number of stations are used). The joint method maintains similarly high performance after merging all datasets and decreasing station coverage to 8 randomly sampled stations (TPR=98.5%, FPR=4.2%). Thus, it promises transportability to other regions of interest with less favorable station coverage. Our proposed metric is suitable for reliable near-real time screening that will benefit regional monitoring and hazard evaluation, as well as future developments of machine-learning based classifiers.

Acknowledgments

All data can be downloaded via the Incorporated Research Institutions for Seismology (IRIS) Data Management Center with catalogs in the supporting information (Table S2): <http://ds.iris.edu/ds/nodes/dmc/data/types/waveform-data/>. The IRIS DMC is supported by the National Science Foundation under Cooperative Support Agreement EAR-1851048. Regional topography used in Figure 1 are requested from the General Bathymetric Chart of the Oceans (GEBCO; <https://www.gebco.net/> last accessed August 2021). We specifically thank Eric Kiser, Lindsay Worthington, Moira Pyle, and Liang Han for the 1-D velocity models. We thank Rigobert Tibi and Chris Young for helpful discussions. The authors are grateful to the principal investigators and field workers involved in the iMUSH, BASE, SPE and SSIP projects. This research was supported by the Air Force Research Lab under contracts FA9453-17-C-0020, FA9453-19-C-0055, FA9453-20-2-0034, and FA9453-21-2-0024.

References

- Anderson, D. N., Walter, W. R., Fagan, D. K., Mercier, T. M., & Taylor, S. R. (2009). Regional multistation discriminants: magnitude, distance, and amplitude corrections, and sources of error. *Bulletin of the Seismological Society of America*, *99*(2A), 794–808. <https://doi.org/10.1785/0120080014>
- Astiz, L., Eakins, J. A., Martynov, V. G., Cox, T. A., Tytell, J., Reyes, J. C., ... & Vernon, F. L. (2014). The Array Network Facility seismic bulletin: Products and an unbiased view of United States seismicity. *Seismological Research Letters*, *85*(3), 576–593. <https://doi.org/10.1785/0220130141>
- Bennett, T. J., & Murphy, J. R. (1986). Analysis of seismic discrimination capabilities using regional data from western United States events. *Bulletin of the Seismological Society of America*, *76*(4), 1069–1086. <https://doi.org/10.1785/BSSA0760041069>
- Bowers, D., & Selby, N. D. (2009). Forensic seismology and the comprehensive nuclear-test-ban treaty. *Annual Review of Earth and Planetary Sciences*, *37*, 209–236. <https://doi.org/10.1146/annurev.earth.36.031207.124143>
- Castro, R. R., Acosta, J. G., Wong, V. M., Perez-Vertti, A., Mendoza, A., & Inzunza, L. (2011). Location of aftershocks of the 4 April 2010 M w 7.2 El Mayor–Cucapah earthquake of Baja California, Mexico. *Bulletin of the Seismological Society of America*, *101*(6), 3072–3080. <https://doi.org/10.1785/0120110112>
- Dempsey, D. E., Cronin, S. J., Mei, S., & Kempa-Liehr, A. W. (2020). Automatic precursor recognition and real-time forecasting of sudden explosive volcanic eruptions at Whakaari, New Zealand. *Nature communications*, *11*(1), 1–8. <https://doi.org/10.1038/s41467-020-17375-2>
- Dokht, R. M., Smith, B., Kao, H., Visser, R., & Hutchinson, J. (2020). Reac-

- tivation of an intraplate fault by mine-blasting events: Implications to regional seismic hazard in Western Canada. *Journal of Geophysical Research: Solid Earth*, 125(6), e2020JB019933. <https://doi.org/10.1029/2020JB019933>
- Douglas, A. (2007). Forensic seismology revisited. *Surveys in Geophysics*, 28(1), 1–31. DOI 10.1007/s10712-007-9018-7
- Fawcett, T. (2006). An introduction to ROC analysis. *Pattern recognition letters*, 27(8), 861–874. <https://doi.org/10.1016/j.patrec.2005.10.010>
- Fisk, M. D., Gray, H. L., & MCCartor, G. D. (1996). Regional event discrimination without transporting thresholds. *Bulletin of the Seismological Society of America*, 86(5), 1545–1558.
- Fuis, G. S., Bauer, K., Goldman, M. R., Ryberg, T., Langenheim, V. E., Scheirer, D. S., ... & Aagaard, B. (2017). Subsurface geometry of the San Andreas fault in southern California: Results from the Salton Seismic Imaging Project (SSIP) and strong ground motion expectations. *Bulletin of the Seismological Society of America*, 107(4), 1642–1662. <https://doi.org/10.1785/0120160309>
- Gulia, L., & P. Gasperini (2021). Contamination of frequency-magnitude slope (b-value) by quarry blasts: An example for Italy, *Seismological Research Letters*. <https://doi.org/10.1785/0220210080>
- Han, L., Hole, J. A., Stock, J. M., Fuis, G. S., Kell, A., Driscoll, N. W., ... & Lázaro-Mancilla, O. (2016). Continental rupture and the creation of new crust in the Salton Trough rift, Southern California and northern Mexico: results from the Salton Seismic Imaging Project. *Journal of Geophysical Research: Solid Earth*, 121(10), 7469–7489. <https://doi.org/10.1002/2016JB013139>
- Hartse, H. E., Taylor, S. R., Phillips, W. S., & Randall, G. E. (1997). A preliminary study of regional seismic discrimination in central Asia with emphasis on western China. *Bulletin of the Seismological Society of America*, 87(3), 551–568.
- Holt, M. M., Koper, K. D., Yeck, W., D’Amico, S., Li, Z., Hale, J. M., & Burlacu, R. (2019). On the portability of M_L – M_C as a depth discriminant for small seismic events recorded at local distances. *Bulletin of the Seismological Society of America*, 109(5), 1661–1673. <https://doi.org/10.1785/0120190096>
- Kim, W. Y., Simpson, D. W., & Richards, P. G. (1993). Discrimination of earthquakes and explosions in the eastern United States using regional high-frequency data. *Geophysical research letters*, 20(14), 1507–1510. <https://doi.org/10.1029/93GL01267>
- Kintner, J. A., Michael Cleveland, K., Ammon, C. J., & Nyblade, A. (2020). Testing a local-distance R_g/S_g discriminant using observations from the Bighorn Region, Wyoming. *Bulletin of the Seismological Society of America*, 110(2), 727–741. <https://doi.org/10.1785/0120190188>
- Koper, K. D., Holt, M. M., Voyles, J. R., Burlacu, R., Pyle, M. L., Wang,

- R., & Schmandt, B. (2021). Discrimination of small earthquakes and buried single-fired chemical explosions at local distances (<150 km) in the Western United States from comparison of local magnitude (M_L) and coda duration magnitude (M_C). *Bulletin of the Seismological Society of America*, 111(1), 558–570. <https://doi.org/10.1785/0120200188>
- Kortström, J., Uski, M., & Tiira, T. (2016). Automatic classification of seismic events within a regional seismograph network. *Computers & Geosciences*, 87, 22–30. <https://doi.org/10.1016/j.cageo.2015.11.006>
- Linville, L., Pankow, K., & Draelos, T. (2019). Deep learning models augment analyst decisions for event discrimination. *Geophysical Research Letters*, 46(7), 3643–3651. <https://doi.org/10.1029/2018GL081119>
- Mackey, K. G., Fujita, K., Gounbina, L. V., Koz'min, B. M., Imaev, V. S., Imaeva, L. P., & Sedov, B. M. (2003). Explosion contamination of the northeast Siberian seismicity catalog: Implications for natural earthquake distributions and the location of the Tanlu fault in Russia. *Bulletin of the Seismological Society of America*, 93(2), 737–746. <https://doi.org/10.1785/0120010196>
- Marzen, R. E., Gaherty, J. B., Shillington, D. J., & Kim, W. Y. (2021). Shaking in the Southeastern United States: Examining earthquakes and blasts in the Central Georgia–South Carolina Seismic Region. *Seismological Research Letters*. <https://doi.org/10.1785/0220210029>
- O'Rourke, C. T., Baker, G. E., & Sheehan, A. F. (2016). Using P/S amplitude ratios for seismic discrimination at local distances. *Bulletin of the Seismological Society of America*, 106(5), 2320–2331. <https://doi.org/10.1785/0120160035>
- O'Rourke, C. T., & Baker, G. E. (2017). A spectrogram-based method of Rg detection for explosion monitoring. *Bulletin of the Seismological Society of America*, 107(1), 34–42. <https://doi.org/10.1785/0120160184>
- Pechmann, J. C., Bernier, J. C., Nava, S. J., & Terra, F. M. (2006). Correction of systematic time-dependent coda magnitude errors in the Utah and Yellowstone National Park region earthquake catalogs, 1981–2001, in Integrated Regional and Urban Seismic Monitoring—Wasatch Front Area, Utah and Adjacent Intermountain Seismic Belt, W. J. Arabasz, R. B. Smith, J. C. Pechmann, K. L. Pankow, and R. Burlacu (Editors), Appendix C, U.S. Geol. Surv. Final Tech. Rept. Cooperative Agreement 04HQAG0014, 137 pp., available at https://earthquake.usgs.gov/cfusion/external_grants/reports/04HQAG0014.pdf (last accessed August 2021).
- Pyle, M. L., & Walter, W. R. (2019). Investigating the effectiveness of P/S amplitude ratios for local distance event discrimination. *Bulletin of the Seismological Society of America*, 109(3), 1071–1081. <https://doi.org/10.1785/0120180256>
- Rabin, N., Bregman, Y., Lindenbaum, O., Ben-Horin, Y., & Averbuch, A. (2016). Earthquake-explosion discrimination using diffusion maps. *Geophysical Journal International*, 207(3), 1484–1492. <https://doi.org/10.1093/gji/ggw348>

- Renouard, A., Maggi, A., Grunberg, M., Doubre, C. and Hibert, C. (2021). Toward false event detection and quarry blast versus earthquake discrimination in an operational setting using semiautomated machine learning. *Seismological Research Letters*. <https://doi.org/10.1785/0220200305>
- Reynen, A., & Audet, P. (2017). Supervised machine learning on a network scale: Application to seismic event classification and detection. *Geophysical Journal International*, 210(3), 1394–1409. <https://doi.org/10.1093/gji/ggx238>
- Richter, C.F (1958). *Elementary Seismology*, W.H. Freeman and Co., San Francisco, California, 768 pp.
- Rodgers, A. J., Walter, W. R., Schultz, C. A., Myers, S. C., & Lay, T. (1999). A comparison of methodologies for representing path effects on regional P/S discriminants. *Bulletin of the Seismological Society of America*, 89(2), 394–408.
- Russell, D. R. (2006). Development of a time-domain, variable-period surface-wave magnitude measurement procedure for application at regional and teleseismic distances, part I: Theory. *Bulletin of the Seismological Society of America*, 96(2), 665–677. <https://doi.org/10.1785/0120050055>
- Scafidi, D., Viganò, A., Ferretti, G., & Spallarossa, D. (2018). Robust picking and accurate location with RSNI-Picker2: Real-time automatic monitoring of earthquakes and nontectonic events. *Seismological Research Letters*, 89(4), 1478–1487. <https://doi.org/10.1785/0220170206>
- Selby, N. D., Marshall, P. D., & Bowers, D. (2012). mb: Ms event screening revisited. *Bulletin of the Seismological Society of America*, 102(1), 88–97. <https://doi.org/10.1785/0120100349>
- Snelson, C. M., Abbott, R. E., Broome, S. T., Mellors, R. J., Patton, H. J., Sussman, A. J., ... & Walter, W. R. (2013). Chemical explosion experiments to improve nuclear test monitoring. *Eos, Transactions American Geophysical Union*, 94(27), 237–239. <https://doi.org/10.1002/2013EO270002>
- Stanley, W. D., Johnson, S. Y., Qamar, A. I., Weaver, C. S., & Williams, J. M. (1996). Tectonics and seismicity of the southern Washington Cascade Range. *Bulletin of the Seismological Society of America*, 86(1A), 1–18.
- Stevens, J. L., & Day, S. M. (1985). The physical basis of *mb:Ms* and variable frequency magnitude methods for earthquake/explosion discrimination. *Journal of Geophysical Research: Solid Earth*, 90(B4), 3009–3020. <https://doi.org/10.1029/JB090iB04p03009>
- Stump, B. W., Hedlin, M. A., Pearson, D. C., & Hsu, V. (2002). Characterization of mining explosions at regional distances: Implications with the international monitoring system. *Reviews of Geophysics*, 40(4), 1011. <https://doi.org/10.1029/1998RG000048>
- Tang, L., Zhang, M., & Wen, L. (2020). Support vector machine classification of seismic events in the Tianshan orogenic belt. *Journal of Geophysical Research:*

- Solid Earth*, 125(1), e2019JB018132. <https://doi.org/10.1029/2019JB018132>
- Taylor, S. R., Denny, M. D., Vergino, E. S., & Glaser, R. E. (1989). Regional discrimination between NTS explosions and western US earthquakes. *Bulletin of the Seismological Society of America*, 79(4), 1142–1176. <https://doi.org/10.1785/BSSA0790041142>
- Tian, D., Yao, J., & Wen, L. (2018). Collapse and earthquake swarm after North Korea’s 3 September 2017 nuclear test. *Geophysical Research Letters*, 45(9), 3976–3983. <https://doi.org/10.1029/2018GL077649>
- Tibi, R. (2021). Discrimination of seismic events (2006–2020) in North Korea using P/Lg amplitude ratios from regional stations and a bivariate discriminant function. *Seismological Research Letters*. 92 (4), 2399–2409. <https://doi.org/10.1785/0220200432>
- Ulberg, C. W., Creager, K. C., Moran, S. C., Abers, G. A., Thelen, W. A., Levander, A., ... & Crosson, R. S. (2020). Local source Vp and Vs tomography in the Mount St. Helens region with the iMUSH broadband array. *Geochemistry, Geophysics, Geosystems*, 21(3), e2019GC008888. <https://doi.org/10.1029/2019GC008888>
- Voyles, J. R., Holt, M. M., Hale, J. M., Koper, K. D., Burlacu, R., & Chambers, D. J. (2020). A new catalog of explosion source parameters in the Utah region with application to M_L – M_C -based depth discrimination at local distances. *Seismological Research Letters*, 91(1), 222–236. <https://doi.org/10.1785/0220190185>
- Walter, W. R., Mayeda, K. M., & Patton, H. J. (1995). Phase and spectral ratio discrimination between NTS earthquakes and explosions. Part I: Empirical observations. *Bulletin of the Seismological Society of America*, 85(4), 1050–1067.
- Walter, W. R., & Taylor, S. R. (2001). A revised magnitude and distance amplitude correction (MDAC2) procedure for regional seismic discriminants: Theory and testing at NTS (No. UCRL-ID-146882). Lawrence Livermore National Lab.(LLNL), Livermore, CA (United States). <https://doi.org/10.2172/15013384>
- Walter, W. R., Dodge, D. A., Ichinose, G., Myers, S. C., Pasyanos, M. E., & Ford, S. R. (2018). Body-wave methods of distinguishing between explosions, collapses, and earthquakes: Application to recent events in North Korea. *Seismological Research Letters*, 89(6), 2131–2138. <https://doi.org/10.1785/0220180128>
- Wang, R., Schmandt, B., & Kiser, E. (2020). Seismic discrimination of controlled explosions and earthquakes near Mount St. Helens using P/S ratios. *Journal of Geophysical Research: Solid Earth*, 125(10), e2020JB020338. <https://doi.org/10.1029/2020JB020338>

Wang, T., Bian, Y., Yang, Q., & Ren, M. (2021). Correction of P/S amplitude ratios for low-magnitude seismic events based on Bayesian kriging method. *Bulletin of the Seismological Society of America*. <https://doi.org/10.1029/2020JB020338>

Worthington, L. L., Miller, K. C., Erslev, E. A., Anderson, M. L., Chamberlain, K. R., Sheehan, A. F., ... & Siddoway, C. S. (2016). Crustal structure of the Bighorn Mountains region: Precambrian influence on Laramide shortening and uplift in north-central Wyoming. *Tectonics*, *35*(1), 208–236. <https://doi.org/10.1002/2015TC003840>

Zeiler, C., & Velasco, A. A. (2009). Developing local to near-regional explosion and earthquake discriminants. *Bulletin of the Seismological Society of America*, *99*(1), 24–35. <https://doi.org/10.1785/0120080045>

References from supporting information

Anderson, M. L., & Myers S. C. (2010). Assessment of regional-distance location calibration using a multiple-event location algorithm. *Bulletin of the Seismological Society of America*, *100*(2), 868–875, <https://doi.org/10.1785/0120090145>

Brocher, T. M. (2005). Empirical relations between elastic wave speeds and density in the Earth's crust. *Bulletin of the seismological Society of America*, *95*(6), 2081–2092. <https://doi.org/10.1785/0120050077>

Kennett, B. L., Engdahl, E. R., & Buland, R. (1995). Constraints on seismic velocities in the Earth from traveltimes. *Geophysical Journal International*, *122*(1), 108–124. <https://doi.org/10.1111/j.1365-246X.1995.tb03540.x>

Kiser, E., Palomeras, I., Levander, A., Zelt, C., Harder, S., Schmandt, B., ... & Ulberg, C. (2016). Magma reservoirs from the upper crust to the Moho inferred from high-resolution V_p and V_s models beneath Mount St. Helens, Washington State, USA. *Geology*, *44*(6), 411–414. <https://doi.org/10.1130/G37591.1>

Tibi, R., Koper, K. D., Pankow, K. L., & Young, C. J. (2018). Discrimination of anthropogenic events and tectonic earthquakes in Utah using a quadratic discriminant function approach with local distance amplitude ratios. *Bulletin of the Seismological Society of America*, *108*(5A), 2788–2800. <https://doi.org/10.1785/0120180024>

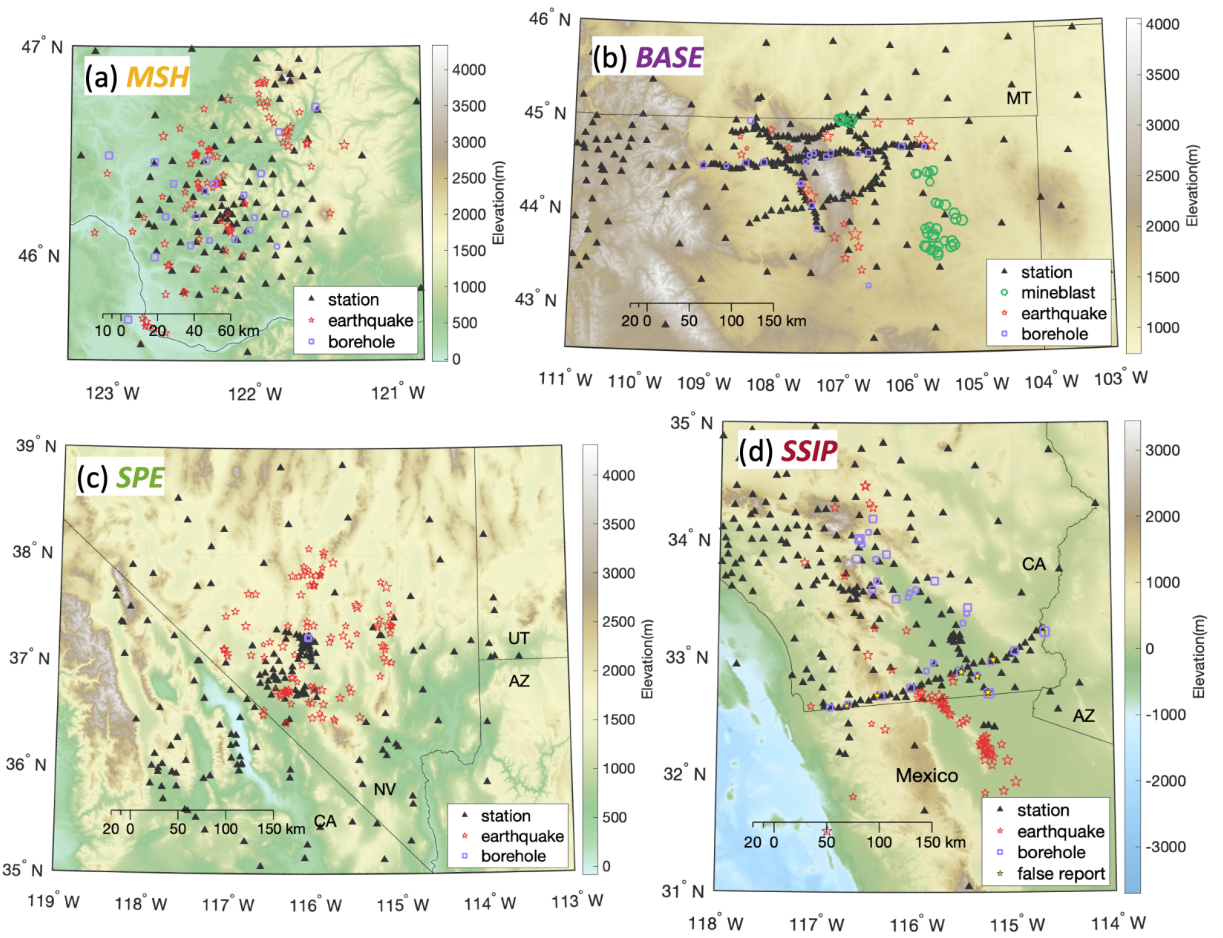


Figure 1. Seismic networks and events for the four studied regions (a–d). See Table S1 for details of the six “false report” earthquakes in SSIP (d).

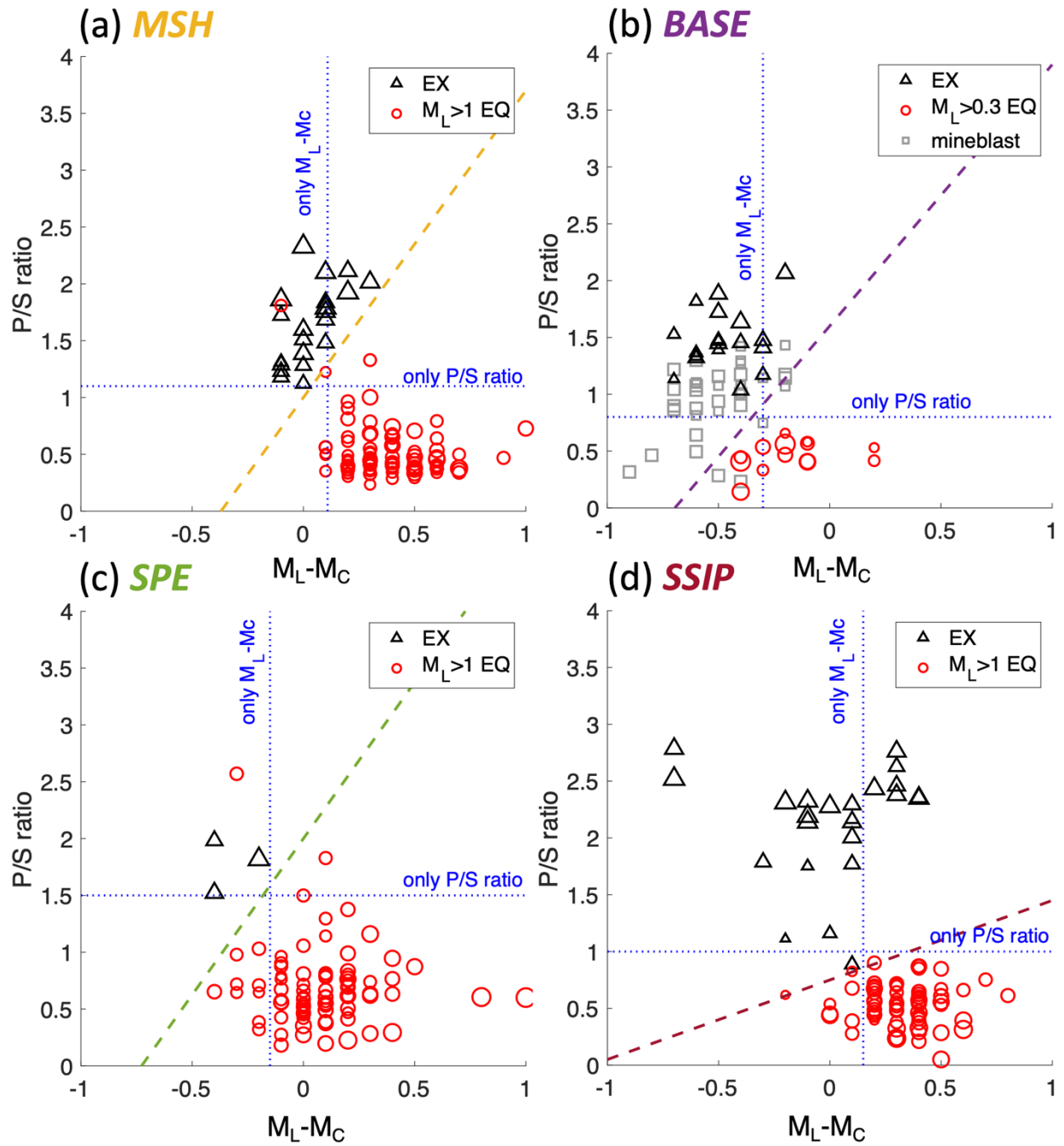


Figure 2. The four datasets analyzed in the joint domain. The horizontal and vertical dotted lines are best P/S ratio and $M_L - M_C$ cutoffs, respectively. The diagonal dashed lines are optional joint cutoffs resolved via grid searching (see

Figure S6). For BASE, the results of 37 mine blasts are shown but excluded from further analysis.

Dataset	MSH	BASE	SPE	SSIP
Neq	90	14	88	70
Nex	22	19	3	22
P/S	1.1	0.9-1.1	1.5	1
TPR (recall)	1	1	1	0.96
FPR	0.03	0	0.02	0
precision	0.88	1	0.60	1
M_L-M_C	0.11	-0.3	-0.15	0.15
TPR (recall)	0.86	0.89	1	0.71
FPR	0.07	0.21	0.11	0.11
precision	0.76	0.85	0.23	0.68
Joint	[2.70 1.00]	[2.30 1.60]	[2.75 2.00]	[0.70 0.75]
TPR (recall)	1	1	1	1
FPR	0.01	0	0.01	0
precision	0.96	1	0.75	1

Table 1. Best discrimination performances for three metrics: 1. P/S; 2. M_L-M_C; and 3. Joint, where numbers in brackets are slope and intercept. For all cases, “explosive” is defined as “positive” (P). True Positive Rate-TPR (recall): TP/(TP+FN); False Positive Rate-FPR: FP/(FP+TN); Precision: TP/(FP+TP). Neq and Nex are final numbers of earthquakes and explosives that have both valid P/S and M_L-M_C measurements.

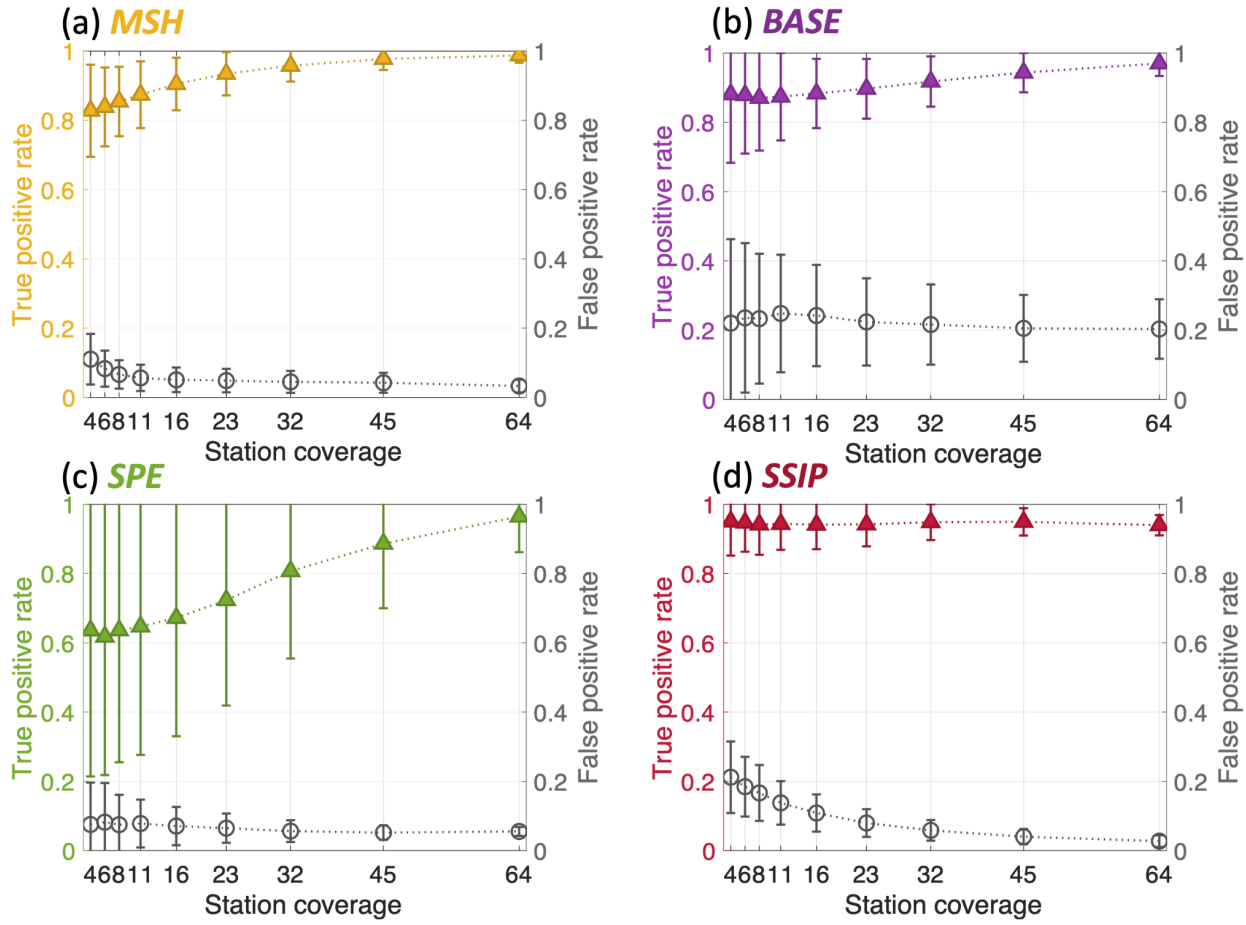
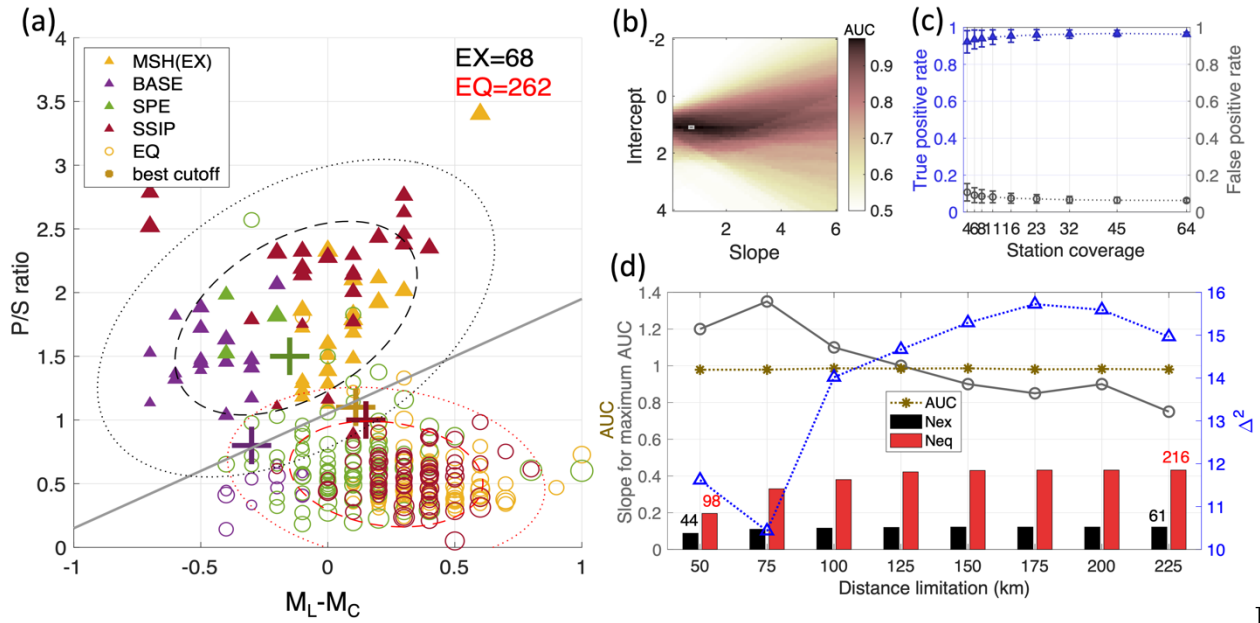


Figure 3. Station coverage test for the four datasets (as labeled). Only broadband stations (i.e., “HH” and “BH”) are considered in BASE. Error bars indicate the standard deviations from 1,000 trials.



4. Discrimination results in the joint domain for merged dataset. (a) All event-based P/S or $M_L - M_C$ of the four datasets as labeled. The cross symbols mark the best P/S and $M_L - M_C$ cut offs for each dataset (see Figure 2). The dashed and dotted ellipses are the covariance of one and two standard deviations, respectively. The grey line marks the best joint discrimination threshold determined from a grid search for maximum AUC shown in (b). (c) Station coverage test for the merged dataset. (d) Slope and discrimination performance variation (Δ^2 and AUC) with source-station distance limitations. Red (Neq) and black (Nex) bars are the numbers of events surviving at each distance limit; only the nearest and farthest distance are labeled with numbers for scaling.